PAPER

Plane-Wave and Vector-Rotation Approximation Technique for Reducing Computational Complexity to Simulate MIMO Propagation Channel Using Ray-Tracing

Wataru YAMADA[†a)], **Naoki KITA**[†], **Takatoshi SUGIYAMA**[†], *and* **Toshio NOJIMA**[††], *Members*

SUMMARY   This paper proposes new techniques to simulate a MIMO propagation channel using the ray-tracing method for the purpose of decreasing the computational complexity. These techniques simulate a MIMO propagation channel by substituting the propagation path between a particular combination of transmitter and receiver antennas for all combinations of transmitter and receiver antennas. The estimation accuracy calculated using the proposed techniques is evaluated based on comparison to the results calculated using imaging algorithms. The results show that the proposed techniques simulate a MIMO propagation channel with low computational complexity, and a high level of estimation accuracy is achieved using the proposed Vector-Rotation Approximation technique compared to that for the imaging algorithm.

key words: *MIMO propagation channel prediction technique, ray-tracing method, imaging algorithm, substitution technique*

1. Introduction

Multiple-Input Multiple-Output (MIMO) systems represented by IEEE802.11n [1] and WiMAX [2] are under investigation as ways to achieve high-speed wireless communications. These MIMO systems are investigated through measurements in actual environments [3] and computer propagation simulations [4] in order to find an appropriate antenna configuration because the configuration significantly affects the data rate of MIMO systems. It is also important to estimate its service area in order to plan wireless systems that use MIMO systems. Therefore, measurement in a real environment [5] and computer propagation simulations [6] were performed to plan its service area. Although there is no doubt that evaluation through measurement in a real environment is the best, it is difficult to use the measurement approach because of cost and time. Therefore, computer propagation simulations prevail as a practical evaluation approach.

There are various propagation simulation methods. The ray-tracing method [7] is one of the most popular simulation methods, especially for evaluating MIMO systems. The ray-tracing method derives propagation paths that are calculated using geometric optics from the transmitter to re-

ceiver. The calculation accuracy can be improved by increasing the number of reflections, diffractions, and penetration. However, the computational complexity increases with the number of walls, reflections, diffraction, and penetration [7]. For instance, in the case of the imaging algorithm, it is necessary to search for the propagation path against the combination of all allocated building walls. So, in the case of Single-Input Single-Output (SISO) systems, it is necessary to judge whether a reflection or diffraction point exists on the wall or diffraction wedge for A^B times in total, when the number of building walls is set to A, and the number of reflections is set to B. Thus, many computational complexity reduction techniques have been studied, for instance [7]–[10]. Evaluations on MIMO propagation channels that use the ray-tracing method were also reported [11]–[14]. However, there is an additional problem in that the computational complexity increases in proportion to the number of combinations of antennas when the ray-tracing method is applied to MIMO systems. For instance, whether a reflection or diffraction point exists on the wall or diffraction wedge for $m \times n \times A^B$ times in total must be judged, when assuming an $m \times n$ MIMO system.

In this paper, two techniques, the Plane-Wave Approximation technique (PWA technique) and Vector-Rotation Approximation technique (VRA technique), are proposed that can simulate a MIMO propagation channel based on the ray-tracing method while reducing the computational complexity. The proposed techniques simulate a MIMO propagation channel by substituting the propagation path between a particular combination of transmitter and receiver antennas for all combinations of antennas. As a result, even when the number of antenna elements is increased, the proposed techniques make it possible to estimate the MIMO propagation channel without increasing the computational complexity.

This paper is organized as follows. In Sect. 2, details of the proposed techniques for simulating a MIMO propagation channel based on the ray-tracing method are given. Next, the proposed techniques are verified based on error analysis in Sect. 3 for single paths. In Sect. 4, an evaluation of the estimation accuracy is presented using a simple simulation model under multipath conditions. Finally, in Sect. 5, we present our conclusions.

2. New Techniques for Simulating MIMO Propagation Channel Using Ray-Tracing

In general, a MIMO propagation channel simulation is performed under the condition that the physical size of the transmitting and receiving array antennas is extremely small compared to the distance between the transmitting and receiving antennas. Under such a condition, the propagation paths between all the transmitter and receiver antenna elements are often extremely analogous. Thus, to decrease the computational complexity, it is thought that a MIMO propagation path can be simulated by substituting the propagation path between a particular combination of antennas for those for all the combinations of transmitter and receiver antennas. However, because the propagation path between actual antenna elements is different from the propagation path between a particular combination of antennas, two techniques are devised as correcting the estimation error of propagation path.

In this section, PWA technique and VRA technique are proposed. Although the PWA technique is used as an approximation technique in array antenna systems [15], this technique is extended to simulate the MIMO propagation channel in this paper. The VRA technique, which yields a more accurate approximation than the PWA technique, is introduced. Procedures for both techniques are illustrated based on the imaging algorithm. Moreover, the computational complexity reduction effects of these techniques are described in this section.

2.1 Definition of Geometrical Terms

In this subsection, the geometrical terms are defined before introducing the proposed techniques. Here, symbols in boldface type represent the position vector, and symbols in boldface italicized type represent the direction vector in this paper. The considered geometry and geometrical terms are illustrated as shown in Fig. 1. Here position $\mathbf{tx_m}$ is the m-th transmitter antenna position, $\mathbf{rx_n}$ is the n-th receiver antenna position, $\mathbf{rx_n^I}$ is the image position of $\mathbf{rx_n}$ with respect to the wall, and $\mathbf{rx_n^V}$, which is derived using the VRA technique, is the substituted image position of $\mathbf{rx_n}$ with respect
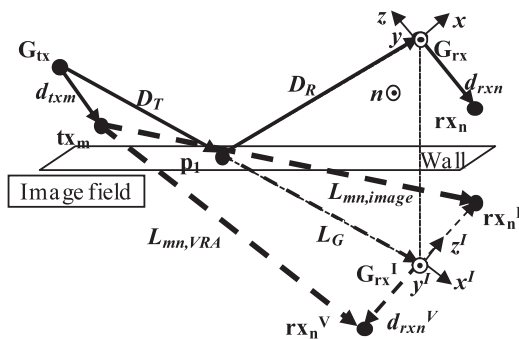

Fig. 1 Definition of geometrical terms.

to the wall. The procedure for deriving $\mathbf{rx_n^V}$ is introduced in Sect. 2.3. Position $\mathbf{G_{tx}}$ is the center of gravity position for the transmitter array, $\mathbf{G_{rx}}$ is the center of gravity position for the receiver array, $\mathbf{G_{rx}^I}$ is the image position of $\mathbf{G_{rx}}$ with respect to the wall, and $\mathbf{p_k}$ is the k-th reflection or diffraction position from $\mathbf{G_{tx}}$ to $\mathbf{G_{rx}}$ for $k = 1, \ldots, K$. Vector $\boldsymbol{d_{txm}}$ is a vector from $\mathbf{G_{tx}}$ to $\mathbf{tx_m}$, $\boldsymbol{d_{rxn}}$ is a vector from $\mathbf{G_{rx}}$ to $\mathbf{rx_n}$, $\boldsymbol{d_{rxn}^V}$ is a vector from $\mathbf{G_{rx}^I}$ to $\mathbf{rx_n^V}$, $\boldsymbol{D_T}$ is a vector from $\mathbf{G_{tx}}$ to $\mathbf{p_1}$, $\boldsymbol{D_R}$ is a vector from $\mathbf{p_K}$ ($\mathbf{p_1}$ in this figure) to $\mathbf{G_{rx}}$, $\boldsymbol{L_G}$ is a vector from $\mathbf{G_{tx}}$ to $\mathbf{G_{rx}^I}$, $\boldsymbol{L_{mn,image}}$ is a vector from $\mathbf{tx_m}$ to $\mathbf{rx_n^I}$, and $\boldsymbol{L_{mn,VRA}}$ is a vector from $\mathbf{tx_m}$ to $\mathbf{rx_n^V}$. Unit vector $\boldsymbol{n}$ is a normal vector of $\mathbf{p_K}$-$\mathbf{G_{rx}}$-$\mathbf{G_{rx}^I}$ plane, unit vector $\boldsymbol{x}$ is set parallel to vector $\boldsymbol{D_R}$, unit vector $\boldsymbol{y}$ is set parallel to vector $\boldsymbol{n}$, and unit vector $\boldsymbol{z}$ is given by Eq. (1).

$$z = y \times x. \tag{1}$$

Furthermore, unit vector $\boldsymbol{x^I}$ is set parallel to vector $\boldsymbol{L_G}$, unit vector $\boldsymbol{y^I}$ is set parallel to vector $\boldsymbol{n}$, and unit vector $\boldsymbol{z^I}$ is given by Eq. (2).

$$z^I = y^I \times x^I. \tag{2}$$

2.2 Proposed PWA Technique for Simulating MIMO Propagation Channel

The PWA technique approximates all the arriving waves as plane waves. In addition, the MIMO propagation channel is calculated by applying the phase difference according to the difference in distance between the transmitter and receiver antenna elements.

2.2.1 Effective Position Allocation Using Ray-Tracing

In the case of the PWA technique, a MIMO propagation channel is simulated by substituting the propagation channel between a particular combination of transmitter and receiver antennas for those for all the combinations of transmitter and receiver antennas. In such a situation, a shorter distance between a particular antenna position and another antenna position is a better situation considering estimation error. So, a desirable antenna position for a particular combination is the center of gravity of transmitter array $\mathbf{G_{tx}}$ and the center of gravity of receiver array $\mathbf{G_{rx}}$. For example, when an m element transmission array antenna is allocated at position $[x_m, y_m, z_m]$, $\mathbf{G_{tx}}$ is calculated using the following equation.

$$\mathbf{G_{tx}} = \left[\frac{\sum_{k=1}^{m} x_k}{m}, \frac{\sum_{k=1}^{m} y_k}{m}, \frac{\sum_{k=1}^{m} z_k}{m} \right]. \tag{3}$$

2.2.2 Procedure and Definition of Propagation Distance and Reflection or Diffraction Angle in PWA Technique

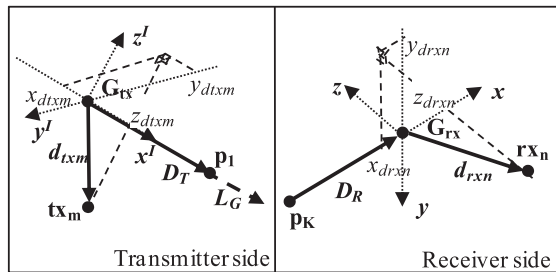A MIMO propagation channel based on the ray-tracing

Fig. 2   Geometrical terms for transmitter and receiver sides.

1. Calculate G_{tx} and G_{rx}.
2. Derive G_{rx}^I against the reflection wall.
3. Calculate the intersection of a straight line that connects G_{rx}^I, G_{tx}, and the wall.
4. Calculate distance x_{dtxm} and x_{drxn}.

Fig. 3   Example of deriving propagation path of one time reflected waves using PWA technique in 2×2 MIMO system.

method is derived using the propagation distance and the reflection or diffraction angle. Therefore, similar to the conventional ray-tracing method, estimating a MIMO propagation channel using the PWA technique requires information regarding the propagation distance and reflection or diffraction angle.

In the PWA technique, the phase difference according to the difference in the distance between the transmitter and receiver antenna elements is applied based on the distance between the plane, which is perpendicular to the vector of the arriving wave, and each antenna position. Figure 2 illustrates the focused geometries of the transmitter and receiver sides shown in Fig. 1.

Here, x_{dtxm}, y_{dtxm}, and z_{dtxm} are the components of d_{txm} in the $x^I y^I z^I$ coordinate system, and x_{drxn}, y_{drxn}, and z_{drxn} are the components of d_{rxn} in the xyz coordinate system. So, d_{txm} and d_{rxn} are expressed as Eqs. (4) and (5), respectively.

$$d_{txm} = x_{dtxm} x^I + y_{dtxm} y^I + z_{dtxm} z^I \text{ and} \tag{4}$$

$$d_{rxn} = x_{drxn} x + y_{drxn} y + z_{drxn} z. \tag{5}$$

In this PWA technique for a MIMO system, x_{dtxm} and x_{drxn} correspond to the phase difference according to the difference in the distance between the transmitter and receiver antenna elements because x_{dtxm} is the distance between the plane which is perpendicular to vector D_T including G_{tx} and tx_m, and x_{drxn} is the distance between the plane which is perpendicular to vector D_R including G_{rx} and rx_n. So, x_{dtxm} and x_{drxn} are calculated for all antenna elements to derive the propagation path of the other antenna combinations. Then, the propagation distance between tx_m and rx_n using the PWA technique, $|L_{mn,PWA}|$, is calculated as indicated below.

$$\left| L_{mn,PWA} \right| = |L_G| + x_{dtxm} + x_{drxn}. \tag{6}$$

Figure 3 shows the procedure for deriving the propagation distance using the PWA technique for a one-time reflected wave in a 2×2 MIMO system. The procedure is given below.

On the other hand, the reflection and diffraction angles in the PWA technique are defined as the same angles that are derived using ray-tracing from G_{tx} to G_{rx}. This is because the propagation paths between all transmitter and receiver antenna elements are often extremely analogous to the results of ray-tracing from G_{tx} to G_{rx}.
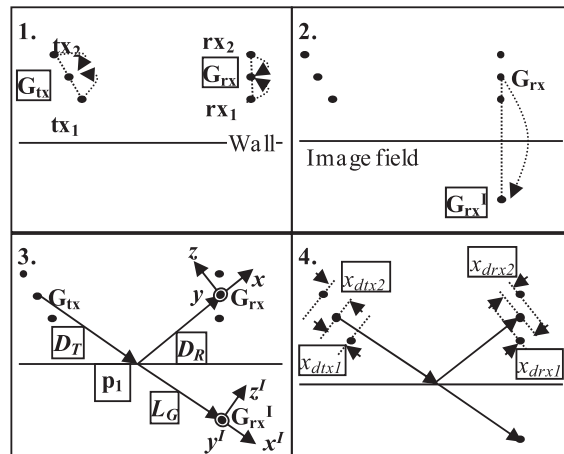
2.2.3   Problem Facing PWA Technique

The problem facing the PWA technique is that the relationship of the actual antenna intervals cannot be considered because the PWA technique approximates the arriving waves as plane waves. For instance, as shown in Eq. (6), the propagation distance between tx_m and rx_n is calculated by vector L_G, x_{dtxm}, and x_{drxn}. Moreover, y_{dtxm}, z_{dtxm}, y_{drxn}, and z_{drxn} are not considered. Therefore, precise $|d_{txm}|$ and $|d_{rxn}|$ as shown in Eqs. (4) and (5) are not affected by using the PWA technique.

2.3   Proposed VRA Technique for Simulating MIMO Propagation Channel

PWA technique proposed in the foregoing subsection assume the difference of propagation distance between the array center of gravity and each array element as a plane wave, and attempt to decrease the estimation error of propagation distance using the difference as a correction value. However, PWA technique cannot fundamentally adjust the estimation error of propagation distance to zero.

The propagation distances for all the antenna combinations are calculated by deriving the image position of all the receiver antenna elements using ray-tracing. To derive strictly accurate distances between antennas, accurate image positions for all the antennas are required. However, since it is necessary to perform the ray-tracing calculation for all the antenna elements, there is a problem in terms of the computational complexity. To address the problem regarding the PWA technique and conventional ray-tracing method, we propose the VRA technique.
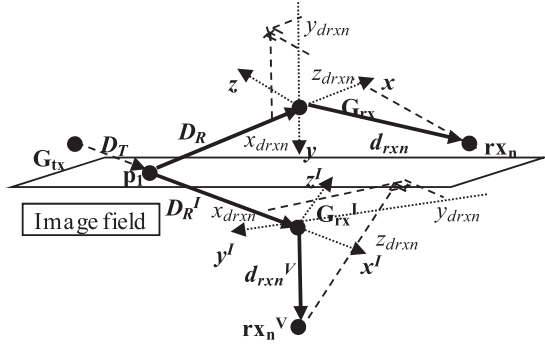
Fig. 4 Geometrical terms for receiver side.

1. Calculate $\mathbf{G_{tx}}$, $\mathbf{G_{rx}}$, vector $\boldsymbol{d_{txm}}$, and vector $\boldsymbol{d_{rxn}}$.
2. Derive $\mathbf{G_{rx}^I}$ against the reflection wall.
3. Calculate the intersection of a straight line that connects $\mathbf{G_{rx}^I}$, $\mathbf{G_{tx}}$, the wall, reflection position $\mathbf{p_1}$, vector $\boldsymbol{D_T}$, and vector $\boldsymbol{D_R}$.
4. Derive the substituted image position $\mathbf{rx_n^V}$.

Fig. 5 Example of deriving propagation path of one time reflected waves using VRA technique in 2×2 MIMO system.
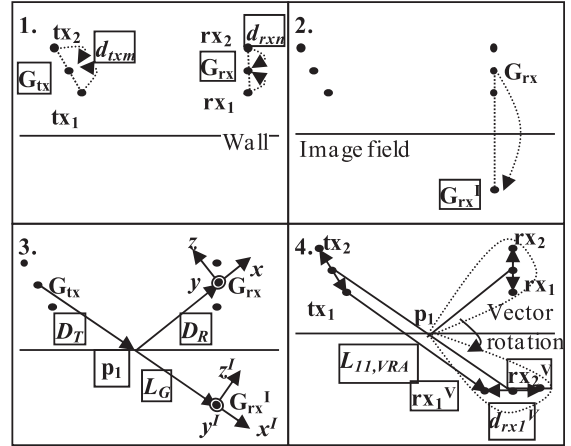
VRA technique attempt to decrease the estimation error of propagation distance using information on the position between the array center of gravity and each array element. In particular, VRA technique doesn't calculate the image position about an individual array element though VRA technique requests the image position of the array center of gravity. And, the position relationship between each element and the array center of gravity is applied to the image position of the array center of gravity. Especially, this VRA technique can suppress the estimation error of propagation distance to zero in the case of simulating Single-Input Multiple-Output (SIMO) and Multiple-Input Single-Output (MISO) propagation channel. The specific calculation method of VRA technique is described as follows.

Figure 4 shows the focused geometry on the receiver side and that for the image field shown in Fig. 1. Here, position $\mathbf{p_k^I}$ represents the k-th reflection or diffraction position from $\mathbf{G_{tx}}$ to $\mathbf{G_{rx}^I}$ in the image field for $k = 1, \ldots, K$, and $\boldsymbol{D_R^I}$ is a vector from $\mathbf{p_K^I}$ to $\mathbf{G_{rx}^I}$ (In this example, $\mathbf{p_1}$ is used instead of $\mathbf{p_K^I}$. Because this example shows the case of a one-time reflected wave, $\mathbf{p_1}$ is identical to $\mathbf{p_1^I}$). The direction of vector $\boldsymbol{D_R^I}$ is equal to the direction of vector $\boldsymbol{D_T}$ because $\mathbf{G_{tx}}$-$\mathbf{G_{rx}^I}$ is a straight line.

As shown in Fig. 4, the VRA method can derive the substituted image positions of all the antennas in the image field. At this time, x_{drxn}, y_{drxn}, and z_{drxn} on the $\boldsymbol{xyz}$ coordinate system are applied to the corresponding $\boldsymbol{x^I y^I z^I}$ coordinate system. In particular, in the VRA technique, the propagation path is first searched using ray-tracing from $\mathbf{G_{tx}}$ to $\mathbf{G_{rx}}$ similar to the case of the PWA technique. In addition, to preserve the position relationship between antenna positions and arriving waves, the same position relationship of the position relationship between the position of the receiving antennas and the last reflection position calculated by ray-tracing between $\mathbf{G_{tx}}$-$\mathbf{G_{rx}}$ is developed in the image field. Therefore, when vector $\boldsymbol{d_{rxn}^V}$ is defined such that the position relationship between vector $\boldsymbol{D_R^I}$ and vector $\boldsymbol{d_{rxn}^V}$ is the same as the position relationship between vector $\boldsymbol{D_R}$ and vector $\boldsymbol{d_{rxn}}$, $\boldsymbol{d_{rxn}^V}$ is shown as Eq. (7).

$$\boldsymbol{d_{rxn}^V} = x_{drxn}\boldsymbol{x^I} + y_{drxn}\boldsymbol{y^I} + z_{drxn}\boldsymbol{z^I}. \tag{7}$$

Position $\mathbf{rx_n^V}$, which is the substituted image position of $\mathbf{rx_n}$ using the VRA technique, is derived by setting $\mathbf{G_{rx}^I}$

as the starting point of vector $\boldsymbol{d_{rxn}^V}$. Since $\mathbf{G_{rx}^I}$ is derived by ray-tracing from $\mathbf{G_{tx}}$ to $\mathbf{G_{rx}}$, $\mathbf{rx_n^V}$ can easily be calculated as Eq. (8).

$$\mathbf{rx_n^V} = \mathbf{G_{rx}^I} + \boldsymbol{d_{rxn}^V}. \tag{8}$$

In the VRA technique for a MIMO system, $\mathbf{rx_n^V}$ is calculated for all receiver antenna elements. When the substituted image positions are fixed, the propagation distance between all the transmitter and receiver antenna elements can be calculated. The propagation distance between $\mathbf{tx_m}$ and $\mathbf{rx_n}$ using the VRA technique, $|L_{mn,VRA}|$, is defined below.

$$\left| L_{mn,VRA} \right| = \left| \boldsymbol{d_{rxn}^V} + \boldsymbol{L_G} - \boldsymbol{d_{txm}} \right|. \tag{9}$$

Thus, to calculate the propagation distance between all the transmitter and receiver antenna elements, the VRA technique requires information on $\mathbf{p_1}$ in order to derive vector $\boldsymbol{L_G}$, and components x_{dtxm}, y_{dtxm}, and z_{dtxm}, and on $\mathbf{p_K}$ in order to derive components x_{drxn}, y_{drxn}, and z_{drxn}.

Figure 5 shows the summarized procedure to derive the propagation distance using the VRA technique for a one-time reflected wave in a 2×2 MIMO system. The procedure is given below.

On the other hand, the reflection and diffraction angles in the VRA technique are defined as the same angles derived using ray-tracing from $\mathbf{G_{tx}}$ to $\mathbf{G_{rx}}$ similar to the case when using the PWA technique.

Figure 6 gives the vision of propagation distance by VRA technique. The sets of image position $\mathbf{rx_n^V}$ derived by the VRA technique form a circle. At this time, the position $\mathbf{rx_n^I}$ is also existing on this circle. In the case of SIMO propagation channel, the right circular cone with the vertex $\mathbf{tx_m}$ and this circle as the base is formed. Therefore, the propagation distances from the position $\mathbf{tx_m}$ to $\mathbf{rx_n^V}$ and the position $\mathbf{tx_m}$ to $\mathbf{rx_n^I}$ are equal. On the other hand, in the case of
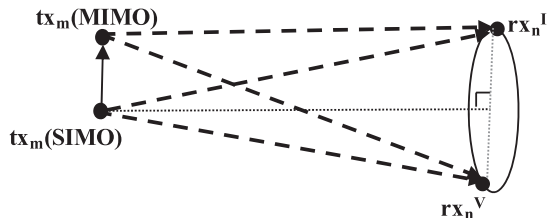
Fig. 6 Propagation distance by VRA technique.

Fig. 7 Example of calculating propagation path using ray-tracing for a two-time reflected wave.

MIMO propagation channel, the position $\mathbf{tx_m}$ departs from the center line because of the physical size of the transmitting array antennas. As a result, the propagation distances from the position $\mathbf{tx_m}$ to $\mathbf{rx_n^V}$ and the position $\mathbf{tx_m}$ to $\mathbf{rx_n^I}$ is slightly different. However, the position $\mathbf{tx_m}$ can approximate to be on the center line, when the physical size of the transmitting array antennas is extremely small compared to the distance between the transmitting and receiving antennas. In this way, from the substituted image positions, an approximate propagation distance can be calculated. However, the fact of the matter is that the real position $\mathbf{tx_m}$ is not on the center line in the case of MIMO propagation channel. Therefore, the propagation distance using the VRA technique includes some error compared to when using the imaging algorithm. In Sects. 3 and 4, the influence of this difference in position is analyzed.

2.4 Effect of Computational Complexity Reduction Using Proposed Techniques

By using the proposed techniques, as the number of antennas increases, the effect from the decrease in the computational complexity increases. This is because the path search process comprises the majority of the computational complexity in the conventional ray-tracing method. For instance, when 4×4 MIMO is assumed, the number of antenna combinations becomes 16. Therefore, the computational complexity using the PWA and VRA techniques becomes approximately 1/16 compared to that for the conventional ray-tracing method.

Because the proposed techniques are the techniques for decreasing the computational complexity of the path search, it is possible to apply these techniques to not only the imaging algorithm but also the ray-launching algorithm. The computational complexity in the ray-launching algorithm can be reduced inverse proportionally to the number of antenna combinations similar to the case of the imaging algorithm. In addition, the proposed techniques further decrease the computational complexity by combining previously proposed ray-tracing acceleration algorithms such as [7]–[10], because these ray-tracing acceleration algorithms are mainly focused on achieving an efficient path search process.

3. Estimation Error Analysis Concerning Single Path

The propagation channels calculated using the ray-tracing method are derived using the propagation distance, reflec-
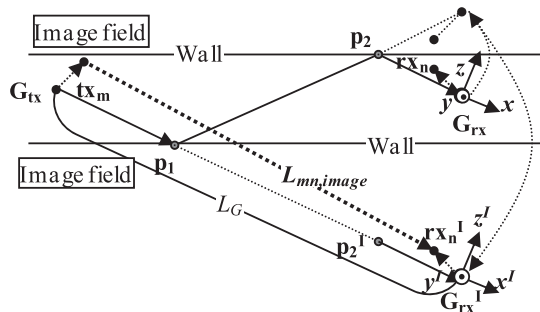
tion or diffraction angle, and electrical property of the wall. The electrical property of the wall is a fixed parameter. On the other hand, since the propagation distance and reflection or diffraction angle calculated by the PWA and VRA are approximated parameters, there is some mismatch between these parameters calculated using the PWA and VRA techniques and the conventional ray-tracing. Therefore, in this section, the propagation distance error and reflection or diffraction angle error for a single path are verified for the PWA and VRA techniques.

3.1 Preparing for Estimation Error Analysis

In this section, the errors are analyzed in an image field. The advantage of using image field analysis is that comprehensive error analysis can be performed because the propagation path between specific positions is converted into a straight line, even though there are multiple reflections or diffractions. A calculation example for a propagation path using ray-tracing for a two-time reflected wave is shown in Fig. 7.

Here, L_G is the distance between $\mathbf{G_{tx}}$ and $\mathbf{G_{rx}^I}$. The propagation path between $\mathbf{G_{tx}}$ and $\mathbf{G_{rx}}$ for a two-time reflection using the ray-tracing method is calculated from $\mathbf{G_{tx}}$ to $\mathbf{G_{rx}}$ through $\mathbf{p_1}$ and $\mathbf{p_2}$. On the other hand, in the image field, it is simply calculated as $\mathbf{G_{tx}}$ to $\mathbf{G_{rx}^I}$, and the propagation path between $\mathbf{tx_m}$ and $\mathbf{rx_n}$ in the image field is calculated as $\mathbf{tx_m}$ to $\mathbf{rx_n^I}$.

We assume that the propagation paths between all transmitter and receiver antenna elements calculated using the conventional ray-tracing method are often extremely analogous. Under this condition, the propagation path at K time reflections and diffractions in the image field can be spread out as shown in Fig. 8. The focused geometries of the transmitter side and receiver side in an image field are shown in Fig. 9.

Here, d_{txm}, and d_{rxn} represent the distance between $\mathbf{G_{tx}}$ and $\mathbf{tx_m}$, and $\mathbf{G_{rx}^I}$ and $\mathbf{rx_n^I}$, respectively. Furthermore, $\boldsymbol{d_{rxn}^I}$ is the vector from $\mathbf{G_{rx}^I}$ to $\mathbf{rx_n^I}$. Angle ϕ_{txm} represents the angle between the orthogonal projection of vector $\boldsymbol{d_{txm}}$ onto the $\boldsymbol{y^I z^I}$-plane and the $\boldsymbol{x^I y^I}$-plane, ϕ_{rxn}^I is the angle between the orthogonal projection of vector $\boldsymbol{d_{rxn}^I}$ onto the $\boldsymbol{y^I z^I}$-plane and the $\boldsymbol{x^I y^I}$-plane, and ϕ_{rxn}^V is the angle between the orthogonal

YAMADA et al.: PLANE-WAVE AND VECTOR-ROTATION APPROXIMATION TECHNIQUE

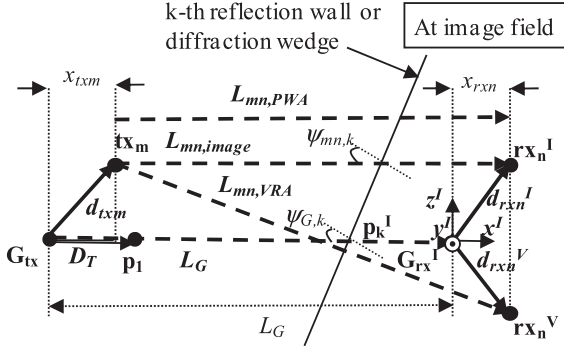**Fig. 8** Image field analysis of propagation path.
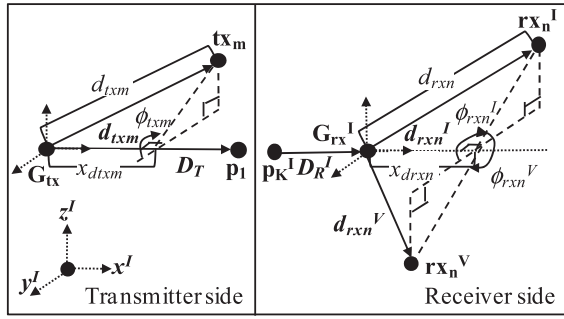
Fig. 9 Focused geometries of transmitter and receiver sides.

projection of vector $\boldsymbol{d}_{rxn}^V$ onto the $\boldsymbol{y^I z^I}$-plane and the $\boldsymbol{x^I y^I}$-plane. These are the anticlockwise azimuth angles from the positive $\boldsymbol{y^I}$-axis and the range of these angles is represented by the interval $[-\pi, \pi)$. Angle $\psi_{G,k}$ represents the incident angle between the k-th reflection wall or diffraction wedge and vector $\boldsymbol{L_G}$, and $\psi_{mn,k}$ represents the incident angle between the k-th reflection wall or diffraction wedge and vector $\boldsymbol{L_{mn,image}}$.

3.2 Estimation Error Analysis for Propagation Distance Using Proposed Techniques

In this subsection, the propagation distance error that arises as a result of applying the PWA and VRA techniques is analyzed. To analyze the propagation distance error, since unit vector $\boldsymbol{x^I}$ is parallel to vector $\boldsymbol{L_G}$ (vector from $\mathbf{G_{tx}}$ to $\mathbf{G_{rx}^I}$), $\boldsymbol{L_{mn,image}}$, $\boldsymbol{L_{mn,PWA}}$, and $\boldsymbol{L_{mn,VRA}}$ are expressed according to Figs. 8 and 9 as

$\boldsymbol{L_{mn,image}}$

$$
= \begin{bmatrix} L_G + x_{dtxm} + x_{drxn} \\ \sqrt{d_{rxn}^2 - x_{drxn}^2}\cos\phi_{rxn}^I - \sqrt{d_{txm}^2 - x_{dtxm}^2}\cos\phi_{txm} \\ \sqrt{d_{rxn}^2 - x_{drxn}^2}\sin\phi_{rxn}^I - \sqrt{d_{txm}^2 - x_{dtxm}^2}\sin\phi_{txm} \end{bmatrix}, \quad (10)
$$

$$
\boldsymbol{L_{mn,PWA}} = \begin{bmatrix} L_G + x_{dtxm} + x_{drxn} \\ 0 \\ 0 \end{bmatrix}, \text{ and} \quad (11)
$$

$\boldsymbol{L_{mn,VRA}}$

$$
= \begin{bmatrix} L_G + x_{dtxm} + x_{drxn} \\ \sqrt{d_{rxn}^2 - x_{drxn}^2}\cos\phi_{rxn}^V - \sqrt{d_{txm}^2 - x_{dtxm}^2}\cos\phi_{txm} \\ \sqrt{d_{rxn}^2 - x_{drxn}^2}\sin\phi_{rxn}^V - \sqrt{d_{txm}^2 - x_{dtxm}^2}\sin\phi_{txm} \end{bmatrix}, \quad (12)
$$

respectively.

Then, $\mathrm{Ed}_{mn,PWA}$ and $\mathrm{Ed}_{mn,VRA}$, which represent propagation distance estimation errors between $\mathbf{tx_m}$ and $\mathbf{rx_n}$ compared to the PWA and VRA techniques for the imaging algorithm, are defined as follows.

$$
\mathrm{Ed}_{mn,PWA} = \left\| |\boldsymbol{L_{mn,image}}| - |\boldsymbol{L_{mn,PWA}}| \right\|
$$
$$
= \left| \begin{array}{l} \sqrt{A_{mn} - B_{mn}\cos(\phi_{txm} - \phi_{rxn}^I)} \\ -(L_G + x_{dtxm} + x_{drxn}) \end{array} \right|, \text{ and} \quad (13)
$$

$$
\mathrm{Ed}_{mn,VRA} = \left\| |\boldsymbol{L_{mn,image}}| - |\boldsymbol{L_{mn,VRA}}| \right\|
$$
$$
= \left| \begin{array}{l} \sqrt{A_{mn} - B_{mn}\cos(\phi_{txm} - \phi_{rxn}^I)} \\ - \sqrt{A_{mn} - B_{mn}\cos(\phi_{txm} - \phi_{rxn}^V)} \end{array} \right|, \quad (14)
$$

respectively.

Here, coefficients A_{mn} and B_{mn} in Eqs. (13) and (14) are defined as follows.

$$
\begin{cases} A_{mn} = L_G^2 - 2(x_{dtxm} + x_{drxn})L_G + 2x_{dtxm}x_{drxn} \\ \qquad\quad + d_{txm}^2 + d_{rxn}^2 \\ B_{mn} = 2\sqrt{d_{rxn}^2 - x_{drxn}^2}\sqrt{d_{txm}^2 - x_{dtxm}^2} \end{cases}. \quad (15)
$$

From Eqs. (14) and (15), we note that the propagation distance estimation error does not occur in the VRA technique when d_{txm} or d_{rxn} is equal to 0 such as in a SIMO or MISO system. This is because in the case of $d_{txm}=0$, since x_{txm} becomes 0, coefficient B_{mn} is equal to 0. On the other hand, a propagation distance estimation error occurs in the PWA technique.

3.2.1 Antenna Position Dependency on Propagation Distance Estimation Error

From Eqs. (13) and (14), the difference of each antenna position is expressed by the angle relationship between ϕ_{txm}, ϕ_{rxn}^I, and ϕ_{rxn}^V, where ϕ_{txm}, ϕ_{rxn}^I, and ϕ_{rxn}^V are angles that represent the position of $\mathbf{tx_m}$, $\mathbf{rx_n^I}$, and $\mathbf{rx_n^V}$, respectively. The propagation distance estimation error is a function of $(\phi_{txm} - \phi_{rxn}^I)$ from Eq. (13). That is, Eq. (13) represents a function of the relative antenna position. On the other hand, the propagation distance estimation error is a function of $(\phi_{txm} - \phi_{rxn}^I)$ and $(\phi_{txm} - \phi_{rxn}^V)$ from Eq. (14). In general, angle ϕ_{rxn}^V is changed due to multiple reflections or diffractions. Then, $|\boldsymbol{L_{mn,image}}| - |\boldsymbol{L_{mn,VRA}}|$ has the maximum positive values when $(\phi_{txm} - \phi_{rxn}^V) = 0$, and has the maximum negative values when $(\phi_{txm} - \phi_{rxn}^V) = -\pi$ or π at each $(\phi_{txm} - \phi_{rxn}^I)$. Furthermore, $|\boldsymbol{L_{mn,image}}| - |\boldsymbol{L_{mn,VRA}}|$ continuously changes between the maximum positive and negative values according to ϕ_{rxn}^V at each $(\phi_{txm} - \phi_{rxn}^I)$. Therefore, the mean value of $\mathrm{Ed}_{mn,VRA}$ also exists at each $(\phi_{txm} - \phi_{rxn}^I)$. The maximum value of $\mathrm{Ed}_{mn,VRA}(\phi_{rxn}^V)$ and the mean value of $\mathrm{Ed}_{mn,VRA}(\phi_{rxn}^V)$ are given below.
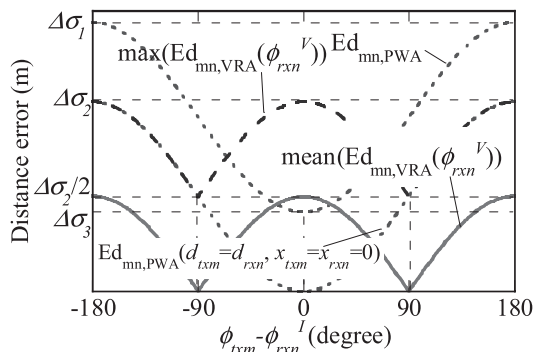
Fig. 10 Dependency of antenna position on propagation distance estimation error.

Fig. 11 Example of maximum distance error of propagation path.

$$\max\left(\mathrm{Ed}_{mn,\mathrm{VRA}}\left(\phi_{rxn}^V\right)\right)$$

$$=\begin{cases}\sqrt{A_{mn}-B_{mn}\cos(\phi_{txm}-\phi_{rxn}^I)}\\ -\sqrt{A_{mn}-B_{mn}}\\ \cdots\left(\omega_{mn}\le\left|\phi_{txm}-\phi_{rxn}^I\right|\le\pi\right)\\ \sqrt{A_{mn}+B_{mn}}\\ -\sqrt{A_{mn}-B_{mn}\cos(\phi_{txm}-\phi_{rxn}^I)}\\ \cdots 0\le\left|\phi_{txm}-\phi_{rxn}^I\right|\le\omega_{mn}\end{cases}, \text{ and}\quad(16)$$

$$\text{mean}\left(\mathrm{Ed}_{mn,\mathrm{VRA}}\left(\phi_{rxn}^V\right)\right)$$

$$=\left|\sqrt{A_{mn}-B_{mn}\cos(\phi_{txm}-\phi_{rxn}^I)}-\sqrt{A_{mn}}\right|.\quad(17)$$

Here, angle ω_{mn} in Eq. (16) is calculated as follows.

$$\omega_{mn}=a\cos\left(\frac{A_{mn}-\sqrt{A_{mn}^2-B_{mn}^2}}{2B_{mn}}\right).\quad(18)$$

In general, since A_{mn} is much larger than B_{mn}, ω_{mn} is approximately $\pi/2$.

Figure 10 shows the antenna position dependency of $\mathrm{Ed}_{mn,\mathrm{PWA}}$ and the maximum and mean values for $\mathrm{Ed}_{mn,\mathrm{VRA}}(\phi_{rxn}^V)$.

In Fig. 10, the solid line represents the mean $\mathrm{Ed}_{mn,\mathrm{VRA}}(\phi_{rxn}^V)$, the dashed line represents the maximum $\mathrm{Ed}_{mn,\mathrm{VRA}}(\phi_{rxn}^V)$, and the dotted line represents $\mathrm{Ed}_{mn,\mathrm{PWA}}$. Furthermore, $\Delta\sigma_1$ is the value of $\max(\mathrm{Ed}_{mn,\mathrm{PWA}})$, $\Delta\sigma_2$ is the value of $\max(\max(\mathrm{Ed}_{mn,\mathrm{VRA}}(\phi_{rxn}^V)))$, and $\Delta\sigma_3$ is the value of $\min(\mathrm{Ed}_{mn,\mathrm{PWA}})$. The values of $\Delta\sigma_1$, $\Delta\sigma_2$, and $\Delta\sigma_3$ change according to d_{txm}, d_{rxn}, x_{txm}, and x_{rxn}. For example, the curve of $\mathrm{Ed}_{mn,\mathrm{PWA}}$ becomes the same curve as the curve of $\max(\mathrm{Ed}_{mn,\mathrm{VRA}}(\phi_{rxn}^V))$ below -90 degrees and above 90 degrees when $d_{txm}=d_{rxn}$, and $x_{txm}=x_{rxn}=0$. At this time, $\Delta\sigma_1$ is equal to $\Delta\sigma_2$ and $\Delta\sigma_3=0$. Therefore, under this condition, the maximum propagation distance estimation error using the VRA technique becomes a large error in the range from -90 to 90 degrees compared to that for the PWA technique. However, in general, the condition when $d_{txm}=d_{rxn}$ and $x_{txm}=x_{rxn}=0$ is a rare case because the delay waves arrive from all directions. In addition, the mean value of $\mathrm{Ed}_{mn,\mathrm{VRA}}(\phi_{rxn}^V)$ is mostly less than that for $\mathrm{Ed}_{mn,\mathrm{PWA}}$. S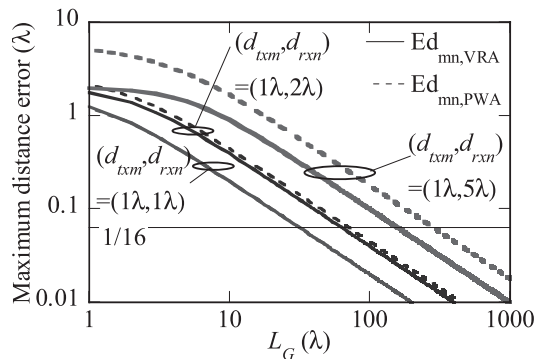o, we can expect that the propagation distance estimation error using the VRA technique is less than that for the PWA technique.

3.2.2 Maximum Propagation Distance Estimation Error

In [16], it is shown that a difference in distance of $\lambda/16$, where λ is the wavelength, is an indication that the propagation distance error can be disregarded. When the maximum error value using some approximation is less than this value for disregarding the error, the approximation can be considered an accurate approximation. Therefore, the maximum propagation distance error is analyzed along with the indication. The maximum propagation distance estimation errors for $\mathrm{Ed}_{mn,\mathrm{PWA}}$ and $\mathrm{Ed}_{mn,\mathrm{VRA}}$ can be calculated from Eqs. (13) and (14), when assuming $L_G\gg x_{dtxm}$ and $L_G\gg x_{drxn}$, respectively.

$$\max\left(\mathrm{Ed}_{mn,\mathrm{PWA}}\right)=\left|\sqrt{L_G^2+(d_{txm}+d_{rxn})^2}-L_G\right|, \text{ and}\quad(19)$$

$$\max\left(\mathrm{Ed}_{mn,\mathrm{VRA}}\right)=\left|\begin{array}{c}\sqrt{L_G^2+(d_{txm}+d_{rxn})^2}\\ -\sqrt{L_G^2+(d_{txm}-d_{rxn})^2}\end{array}\right|.\quad(20)$$

From Eqs. (19) and (20), the maximum propagation distance error becomes the same value using the PWA technique and VRA technique, when $d_{txm}=d_{rxn}$. An example of calculating $\max(\mathrm{Ed}_{mn,\mathrm{VRA}})$ and $\max(\mathrm{Ed}_{mn,\mathrm{PWA}})$ for $(d_{txm}, d_{rxn})=(1\lambda, 1\lambda), (1\lambda, 2\lambda), (1\lambda, 5\lambda)$ is shown in Fig. 11. Here, distance $\lambda/16$, which is an indication that the propagation distance error can be disregarded, is also shown.

In Fig. 11, the solid line represents $\max(\mathrm{Ed}_{mn,\mathrm{VRA}})$, and the dashed line represents $\max(\mathrm{Ed}_{mn,\mathrm{PWA}})$. When the array size is set to $(d_{txm}, d_{rxn})=(1\lambda, 1\lambda), (1\lambda, 2\lambda), (1\lambda, 5\lambda)$, the distance between the transmitter and receiver arrays such that the propagation distance error can be disregarded is over 32λ, 72λ, and 290λ in the PWA technique, and over 32λ, 64λ, and 160λ in the VRA technique. Since the maximum error in the propagation distance using the VRA technique is less than that using the PWA technique in all cases, the advantage of the VRA technique is shown. Furthermore, in a common simulation environment for a MIMO propagation channel, the influence that the VRA technique exerts on the propagation path is extremely small.

3.3 Estimation Error of Reflection or Diffraction Angle Using Proposed Techniques

In the PWA and VRA techniques, it is assumed that all reflection or diffraction angles assume the same angles calculated by the imaging algorithm between $\mathbf{G_{tx}}$ and $\mathbf{G_{rx}}$. So, the reflection or diffraction angle error compared to that for the imaging algorithm with the VRA technique and PWA technique is the same value. The difference between $\psi_{G,k}$ and $\psi_{mn,k}$ corresponds to the difference in the angle between $\mathbf{L_G}$ and $\mathbf{L_{mn,image}}$. Therefore, E$\psi_{mn,k}$, which is the reflection or diffraction angle of the k-th reflection wall or diffraction wedge error between $\mathbf{tx_m}$ and $\mathbf{rx_n}$ by the proposed techniques, is defined as follows.

$$
\begin{aligned}
E\psi_{mn,k} &= \left| \psi_{G,k} - \psi_{mn,k} \right| \\
&= \left| \mathrm{acos}\left(\frac{\mathbf{L_{mn,image}} \cdot \mathbf{L_G}}{|\mathbf{L_{mn,image}}| |\mathbf{L_G}|} \right) \right| \\
&= \mathrm{acos}\left(\frac{L_G + x_{txm} + x_{rxn}}{\sqrt{A_{mn} - B_{mn}\cos(\phi_{txm} - \phi_{rxn}^I)}} \right).
\end{aligned}
\tag{21}
$$

The maximum reflection or diffraction angle error is calculated in the following equation, when assuming $L_G \gg x_{txm}$ and $L_G \gg x_{rxn}$.

$$
\max(E\psi_{mn,k}) = \left| \mathrm{atan}\left(\frac{d_{txm} + d_{rxn}}{L_G} \right) \right|.
\tag{22}
$$

In Fig. 12, $\max(E\psi_{mn,k})$ for $d_{txm} + d_{rxn} = 1\lambda, 2\lambda, 5\lambda$ is shown as a calculation example.

In Fig. 12, the solid line represents $d_{txm} + d_{rxn} = 1\lambda$, the dashed line represents $d_{txm} + d_{rxn} = 2\lambda$, and the dotted line represents $d_{txm} + d_{rxn} = 5\lambda$. This figure shows that $\max(E\psi_{mn,k})$ increases according to the increase in $d_{txm} + d_{rxn}$. However, $\max(E\psi_{mn,k})$ can achieve below 3 degrees, when L_G is over 100λ even in the case of $d_{txm} + d_{rxn} = 5\lambda$. Note that the error shown in this figure is the maximum angle error, so practically, the error becomes smaller than the value indicated here in many cases. However, in a general simulation environment for a MIMO propagation 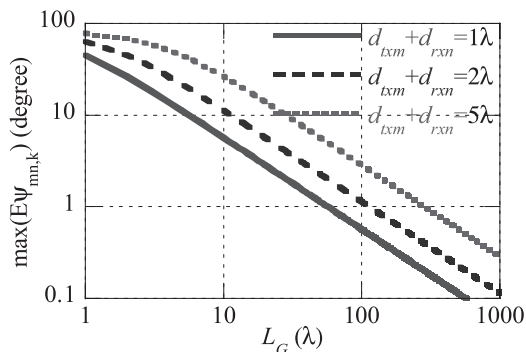channel, the influence that the proposed techniques exert on the propagation channel is extremely small, even in the situation that the reflection or diffraction angle selects the maximum error. This is because this maximum angle error is extremely small.

4. Performance Evaluation

Up to now, the propagation distance error and the reflection or diffraction angle error have been analyzed using the PWA and VRA technique. In this section, simulations of a MIMO propagation channel using the imaging algorithm, PWA technique, and VRA technique are performed to evaluate more general propagation characteristics of a MIMO system using a simple outdoor simulation model under multipath conditions. The evaluation parameter is an eigenvalue calculated from the MIMO correlation matrix because the parameter well reflects the effect of the phase difference of each element. The MIMO propagation channel estimation error is evaluated according to the difference between the eigenvalue calculated using the imaging algorithm and that using the PWA and VRA technique.

4.1 Simulation Model and Simulation Conditions

Simulation of a MIMO propagation channel is performed using the outdoor simulation model shown in Fig. 13, and Table 1 summarizes the simulation conditions. Here, d_T and d_R represent the antenna interval for the transmitter and receiver array, respectively.

In this simulation model, the street microcell environment with 5 to 6 story building was assumed. There are four buildings, the height of the buildings is set to 20 m for this simulation model. The width of the building is set to 10 m. The building material is concrete the complex permittivity of which is $7.00 - j0.85$ [17]. The road is also made of concrete. A four element transmitter antenna array is used for this simulation, and each transmitter antenna position is arranged in a Uniform-Circular-Array (UCA). The height of the transmitter antenna array is set to 3.5 m. A four element
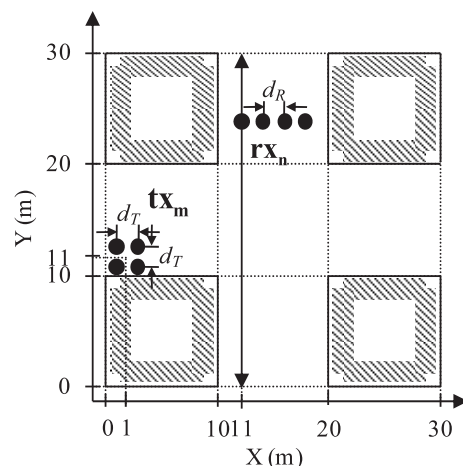

Fig. 12 Example of maximum reflection or diffraction angle error.

Fig. 13 Outdoor simulation model.

Table 1 Simulation conditions.

Frequency	2.45 GHz
Building material	Concrete (complex permittivity: 7.00-j0.85)
Maximum number of reflections	3
Maximum number of diffractions	1
Antenna polarization	Vertical
Antenna interval of transmitter	Case 1 : d_T=0.06 m, Case 2 : d_T=0.6 m
Location of transmitter	1.0 m apart from the building
Height of transmitter	3.5 m
Antenna interval of receiver	Case 1 : d_R=0.03 m, Case 2 : d_R=0.3 m
Location of receiver	1.0 m apart from the building
Height of receiver	1.0 m

Fig. 14 Cumulative probability distribution of eigenvalues (Case 1).

Fig. 15 Cumulative probability distribution of eigenvalues (Case 2).

receiver antenna array is used, and each receiver antenna position is arranged in a Uniform-Linear-Array (ULA). The height of the receiver antenna array is set to 1.0 m. A vertically polarized isotropic antenna is assumed for all transmitter and receiver antennas. There are two cases considered for the antenna position, Case 1 and Case 2.

As shown in Fig. 13, 4 × 4 MIMO propagation characteristics are calculated using the imaging algorithm, PWA technique, and VRA technique in the position from $Y = 0$ m to 30 m at intervals of 1 cm. The calculated frequency is 2.45 GHz. At this frequency, the antenna interval for the transmitter UCA corresponds to 0.5λ for Case 1 and 5λ for Case 2, and the antenna interval for the receiver ULA corresponds to 0.25λ for Case 1 and 2.5λ for Case 2. The maximum number of reflections is set to three, and the number of diffractions is set to one. The reflection coefficient is calculated using the Fresnel reflection coefficient [18] and the diffraction coefficient is calculated using the uniform geometrical theory of diffraction [19]. Here, only the reflected wave and the diffracted wave have been treated as a simulation model for the verification of the proposed techniques. When the propagation characteristic is simulated using ray-tracing method, penetration wave might have to be considered. However, these proposed techniques are effective even in a existence of penetration wave.

4.2 Simulation Results

For this simulation model and conditions, the rate of calculation reduction relative to conventional ray-tracing method is 93.72% for the PWA technique and 93.70% for the VRA technique. The rate of theoretical limitation of the computational complexity reduction is 93.75% when 4 × 4 MIMO propagation channel is simulated by using these proposal techniques. Therefore, these proposal techniques can achieve almost near the percentage of theoretical limitation
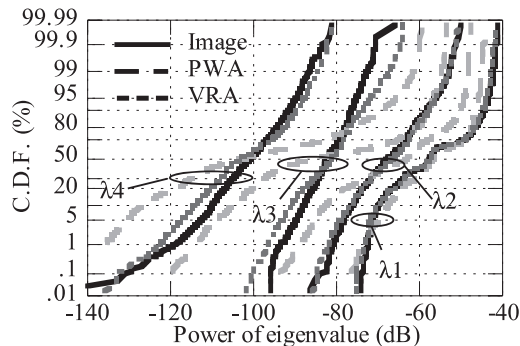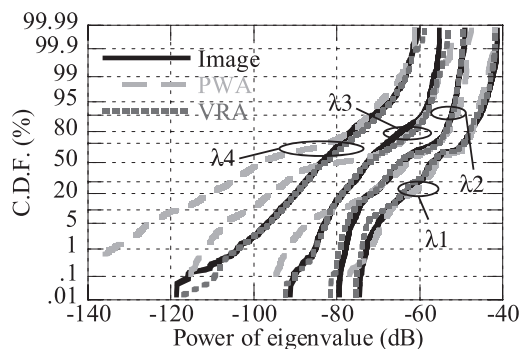
of the computational complexity reduction. Therefore, these results show that the computational complexity for calculating the MIMO propagation channel can be significantly reduced by using the proposed techniques.

Figures 14 and 15 show the cumulative probability of each eigenvalue in the whole simulation section calculated using the imaging algorithm, PWA technique, and VRA technique. Figure 14 is for Case 1, and Fig. 15 is for Case 2.

Here, the solid line represents the imaging algorithm, the dashed line represents the PWA technique, and the dotted line represents the VRA technique. Furthermore, λx represents the x-th biggest eigenvalue calculated using the MIMO correlation matrix. Figures 14 and 15 show that the distribution is almost the same for all eigenvalues compared to that for the imaging algorithm and VRA technique, while a distribution error occurs compared to the imaging algorithm and PWA technique. Therefore, it is shown that a statistical evaluation of the MIMO propagation characteristics calculated using the imaging algorithm cannot be reproduced using the PWA technique, but it is possible using the VRA technique.

Figure 16 shows an example of the eigenvalue variability characteristics using the imaging algorithm, PWA technique, and VRA technique from $Y = 20$ m to 21 m in this simulation model for Case 1.

Here, the solid line represents the imaging algorithm, the dashed line represents the PWA technique, and the dotted line represents the VRA technique. As shown in the figure, the value of each eigenvalue calculated using the imag-
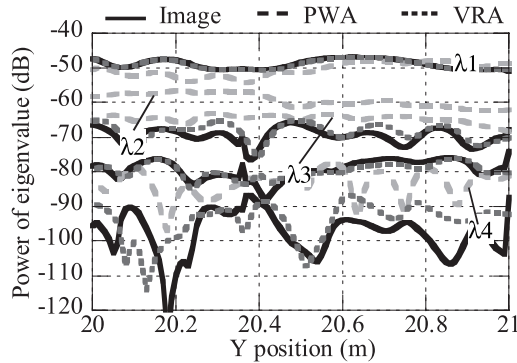
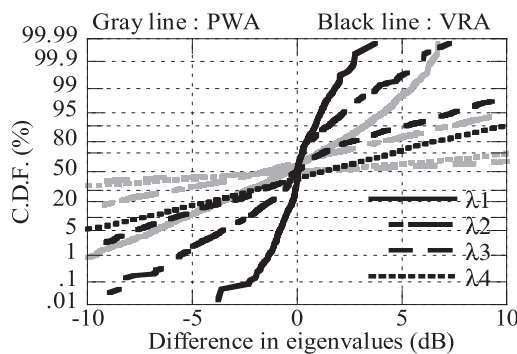**Fig. 16** Example of eigenvalue distance characteristics (Case 1).

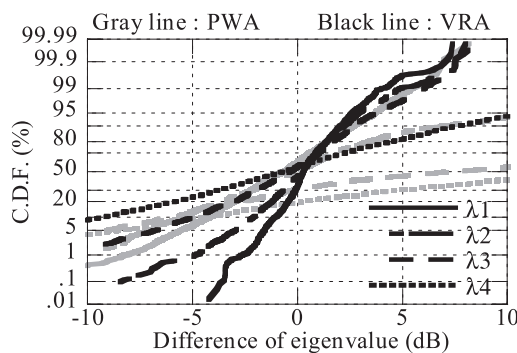**Fig. 17** Error distribution of eigenvalues (Case 1).

Fig. 18 Error distribution of eigenvalues (Case 2).

ing algorithm can be traced using the VRA technique while the eigenvalue obtained using the PWA technique cannot be re-traced in the same position.

Figures 17 and 18 show the cumulative probability for the difference among the eigenvalues calculated using the imaging algorithm compared to those calculated using the PWA technique and VRA technique for the same positions. Figure 17 is for Case 1, and Fig. 18 is for Case 2. From Fig. 17, the error of the eigenvalue using the PWA technique is within 7 dB for $\lambda 1$, within 15 dB for $\lambda 2$, within 25 dB for $\lambda 3$, and within 30 dB for $\lambda 4$ at the cumulative probability of 90%. On the other hand, the error of the eigenvalue using the VRA technique is within 2 dB for $\lambda 1$, within 4 dB for $\lambda 2$, within 8 dB for $\lambda 3$, and within 20 dB for $\lambda 4$ at the cumulative

probability of 90%. From Fig. 18, the error of the eigenvalue using the PWA technique is within 6 dB for $\lambda 1$, within 12 dB for $\lambda 2$, within 25 dB for $\lambda 3$, and within 35 dB for $\lambda 4$ at the cumulative probability of 90%. On the other hand, the error of the eigenvalue using the VRA technique is within 3 dB for $\lambda 1$, within 3 dB for $\lambda 2$, within 4 dB for $\lambda 3$, and within 14 dB for $\lambda 4$ at the cumulative probability of 90%. So, the results show that the proposed VRA technique can simulate a MIMO propagation channel more accurately than when using the PWA technique in each case.

5. Conclusion

In this paper, the VRA and PWA techniques, which are techniques for simulating a MIMO propagation channel based on the ray-tracing method and can address the problem of computational complexity facing the conventional ray-tracing method, were proposed. It was shown that the simulation of a MIMO propagation channel using the imaging algorithm can be traced with high accuracy and low computational complexity using the proposed techniques.

The proposed techniques were verified based on error analysis for a single path. It was shown that the maximum propagation distance estimation error can be disregarded at the distance between the transmitter and receiver arrays of over 160λ for the VRA technique when $(d_{txm}, d_{rxn}) = (1\lambda, 5\lambda)$. Furthermore, the reflection or diffraction angle error compared to that for the imaging algorithm with the VRA technique can achieve below 3 degrees when the distance between the transmitter and receiver array is over 100λ even in the case when $d_{txm} + d_{rxn} = 5\lambda$. Therefore, in a general simulation environment of a MIMO propagation channel, the VRA technique only very slightly influences the propagation channel. The eigenvalues for the imaging algorithm and the proposed techniques were compared to verify the accuracy of the MIMO propagation channel estimation in an outdoor simulation model in the presence of multipaths. It was shown that the statistical characteristics of the eigenvalue calculated using the imaging algorithm and that using the VRA technique are in good agreement for all the eigenvalues. In addition, it was shown that the error of the first eigenvalue $\lambda 1$, which was compared to that for the imaging algorithm for the same transmitter and receiver antenna position, is within 3 dB at the cumulative probability of 90% for the proposed VRA technique. Therefore, the proposed VRA technique was verified to simulate a MIMO propagation channel with low computational complexity and a high level of accuracy.

References

[1] http://ieeexplore.ieee.org/ISOL/standardstoc.jsp?punumber=4360106

[2] IEEE Standard for Local and metropolitan area networks Part 16: Air Interface for Fixed and Mobile Broadband Wireless Access Systems Amendment 2: Physical and Medium Access Control Layers for Combined Fixed and Mobile Operation in Licensed Bands and Corrigendum 1, IEEE Std 802.16e-2005 and IEEE Std 802.16-2004/

Cor 1-2005, 2006.

[3] H. Nishimoto, Y. Ogawa, T. Nishimura, and T. Ogane, "Performance evaluation of 2×2 MIMO space division multiplexing based on indoor propagation measurement," IEICE Trans. Commun. (Japanese Edition), vol.J87-B, no.9, pp.1442–1453, Sept. 2004.

[4] F. Tila, P.R. Shepherd, and S.R. Pennock, "Theoretical capacity evaluation of indoor micro- and macro-MIMO systems at 5 GHz using site specific ray tracing," Electron. Lett., vol.39, no.5, pp.471–472, March 2003.

[5] W. Yamada, N. Kita, A. Ando, and T. Ito, "MIMO channel characteristics using directional antennas for transmission between base station in a street micro-cell environment at 5.2-GHz band, and prediction method for its propagation characteristics," IEICE Trans. Commun. (Japanese Edition), vol.J91-B, no.3, pp.260–271, March 2008.

[6] T. Zwick, C. Fischer, and W. Wiesbeck, "A stochastic multipath channel model including path directions for indoor environment," IEEE J. Sel. Areas Commun., vol.20, no.6, pp.1178–1192, Aug. 2002.

[7] F. Agelet, A. Formella, J. Rabanos, F. Vicente, and F. Fontan, "Efficient ray-tracing acceleration technique for radio propagation modeling," IEEE Trans. Veh. Technol., vol.49, no.6, pp.2089–2104, Nov. 2000.

[8] G. Liang and H.L. Bertoni, "A new approach to 3D ray tracing for propagation prediction in cities," IEEE Trans. Antennas Propag., vol.46, no.6, pp.853–863, June 1998.

[9] T. Imai, "Novel ray-tracing acceleration technique using genetic algorithm for radio propagation prediction," NTT Review, vol.6, no.2, Feb. 2008, https://www.ntt-review.jp/archive/ntttechnical.php?contents=ntr200802le1.html

[10] T. Imai and T. Fujii, "Fast algorithm for indoor microcell area prediction system using ray-tracing method," Electron. Commun. Jpn. 1, Commun., vol.85, no.6, pp.41–52, June 2002.

[11] S. Loredo, A.R. Alonso, and R.P. Torres, "Indoor MIMO channel modeling by rigorous GO/UTD-based ray tracing," IEEE Trans. Veh. Technol., vol.57, no.2, pp.680–692, March 2008.

[12] K.H. Ng, E.K. Tameh, M.H. Hunukumbure, and A.R. Nix, "Efficient multielement ray tracing with site-specific comparisons using measured MIMO channel data," IEEE Trans. Veh. Technol., vol.56, no.3, pp.1019–1032, May 2007.

[13] S. Takahashi, C.J. Ahn, and H. Harada, "Stochastic method of determining substream modulation levels for MIMO eigenbeam space division multiplexing," IEICE Trans. Commun., vol.E89-B, no.1, pp.142–149, Jan. 2006.

[14] D. Gesbert, H. Bolcskei, D.A. Gore, and A.J. Pauraj, "Outdoor MIMO wireless channels: Models and performance prediction," IEEE Trans. Commun., vol.50, no.12, pp.1926–1934, Dec. 2002.

[15] K. Haneda, J. Takada, and T. Kobayashi, "Cluster properties investigated from a series of ultrawideband double directional propagation measurements in home environments," IEEE Trans. Antennas Propag., vol.54, no.12, pp.3778–3788, Dec. 2006.

[16] J.D. Kraus, Antennas, McGraw-Hill, New York, 1988.

[17] Rec. ITU-R P. 1238, "Propagation data and prediction models for the planning of indoor radiocommunication systems and radio local area networks in the frequency range 900 MHz to 100 GHz," ITU-R Recommendations, vol.1997, P Series-Part 2, pp.252–261, ITU, Geneva, 1998.

[18] O. Landron, M.J. Feuerstein, and T.S. Rappaport, "A comparison of theoretical and empirical reflection coefficients for typical exterior wall surfaces in a mobile radio environment," IEEE Trans. Antennas Propag., vol.44, no.3, pp.341–351, March 1996.

[19] R.G. Kouyoumjian and P.H. Pathak, "A uniform geometrical theory of diffraction," Proc. IEEE, vol.62, pp.1448–1461, 1971.

Wataru Yamada received his B.E. and M.E. degrees from Hokkaido University in Japan in 2000 and 2002, respectively. Since joining NTT in 2002, he has been engaged in the research of propagation characteristics for short range wide band access systems. He is now a member of the Wireless Access Systems Laboratories. He received the Young Researcher's Award from the Institute of Electronics, Information and Communication Engineers (IEICE) in 2006. He is a member of the IEEE.

Naoki Kita received his B.E. degree from Tokyo Metropolitan Institute of Technology in Japan in 1994, and received his M.E. and Ph.D. degrees from Tokyo Institute of Technology in Japan in 1996 and 2007, respectively. Since joining NTT in 1996, he has been engaged in the research of propagation characteristics for short range wide band access systems. He is now a senior research engineer of the Wireless Access Systems Project in the NTT Access Network Service Systems Laboratories. He received the Young Researcher's Award from the Institute of Electronics, Information and Communication Engineers (IEICE) in 2002. He is a member of the IEEE.

Takatoshi Sugiyama received the B.E., M.E. and Ph.D. degrees from Keio University, Japan in 1987, 1989 and 1998, respectively. Since joining NTT in 1989, he had been engaged in the research and development of forward error correction, interference compensation, CDMA, modulation-demodulation, MIMO-OFDM technologies for wireless communication systems such as satellite, wireless ATM, wireless LAN systems. From 1988 to 2001, he was in charge of business planning of international satellite communication services in NTT Communications Corporation. From 2004 to 2007, he was in Wireless Laboratories of NTT DoCoMo, Inc., where he worked for the research and development of wireless resource management schemes, plug-and-play base stations and wireless mesh networks. He is currently a senior research engineer, supervisor in NTT Access Network Service Systems Laboratories responsible for the research and development of intelligent interference compensation technologies and radio propagation modeling for future wireless communication systems. He received the Young Engineers Award from the IEICE of Japan in 1996. He is a member of the IEEE.

Toshio Nojima received the B.E. degree in electrical engineering from Saitama University, Saitama, Japan, in 1972, and the M.E. and Ph.D. degrees in electronic engineering from Hokkaido University, Sapporo, Japan, in 1974 and 1988, respectively. From 1974 to 1992, he was with Nippon Telegraph and Telephone (NTT) Communications Laboratories, where he was engaged in the development of high capacity microwave relay systems (SSB-AM and 256QAM systems). From 1992 to 2001, he was with NTT DoCoMo, Inc., where he was a Senior Executive Research Engineer and pursued researches on the radio safety issues of microwave exposures as well as high efficiency radio equipment technologies. Since January of 2002, he has assumed the position of Professor in the graduate school of Hokkaido University. He is a member of the IEEE, the Bioelectromagnetics Society (BEMS).